High-Fidelity 3D Printing of Programmable Magnetic Soft Robots

Siwen Xie[1*], Kaitlyn Clancy[2*], and Onaizah Onaizah[1,2]

***Abstract*— Magnetic microrobots are an increasingly popular area of research with a wide range of potential applications including healthcare. These microrobots can be remotely controlled using an external magnetic field to perform various motions such as jumping, swimming, crawling, rolling, and grabbing. This allows for intricate tasks such as drug delivery, stent placements, and wound patching. However, fabricating microrobots is a challenging multi-step process that can take several hours or even days. Therefore, it is important to have an accurate, reproducible, and automated fabrication method. In this study, an existing fully automated stereolithography printer is tested to fabricate magnetic soft robots with voxel sizes smaller than a millimeter. The work focuses on updating the optics to create a smaller spot size (803 μm) with more uniform curing distributions using a near ultraviolet beam shaper. The updated optics system in the printer is then used to print two microrobots: 'the beam' and 'the gripper' that are functionally tested using an externally applied magnetic field.**

I. INTRODUCTION

Microrobots are an increasingly attractive area of research due to their ability to access small spaces and perform tasks that were previously infeasible. However, their small size limits the integration of on board power systems and electronics, which necessitates remote actuation. Magnetic actuation is a widely adopted approach, as magnetic fields can penetrate most environments and are generally safe for human interaction. This technique requires the use of magnetically responsive materials.

Magnetic soft robots (MSRs) achieve this functionality by embedding magnetic microparticles within a polymer matrix. Since they are primarily composed of polymer-based materials, MSRs benefit from several key advantages, including high flexibility, deformability, and tunable mechanical properties [1]. The integration of magnetic materials, such as neodymium iron boron microparticles (NdFeB) or iron oxide (Fe_3O_4) nanoparticles, enables precise control of microrobot motion when subjected to external magnetic fields [2].

The combination of soft polymers and magnetic particles gives MSRs several desirable properties: high mechanical compliance, strong actuation forces, rapid response times, programmable deformation, and the ability to operate remotely [3]–[8]. As a result, MSRs can effectively navigate complex, narrow and tortuous environments such as blood vessels inside the body to perform tasks like minimally invasive surgery [9], targeted drug delivery [10], and tissue engineering [11].

Despite these promising attributes, MSR fabrication remains a challenge. Current techniques struggle with achieving fabrication precision, producing complex geometries, and optimizing magnetization profiles [12]. Addressing these issues is critical for advancing MSR functionality and real-world applicability.

Traditional microrobot fabrication methods can include electrochemical deposition [13], [14], physical vapor deposition [15], [16], material self-assembly [17], and biohybrid technology [18]. While these methods can satisfy certain application requirements, they are usually complex, time-consuming, labor-intensive, and difficult to customize [19].

In contrast, three-dimensional (3D) printing has emerged as a cost-effective additive manufacturing technology with high automation, repeatability, and customization. It can rapidly accelerate progress in the field of microrobotics by scaling the production rates. The core principle of 3D printing is to deposit material layer-by-layer to construct 3D structures with complex geometries. This process typically uses computer-aided design (CAD) and computer-aided manufacturing (CAM) systems to achieve precise control of the printing path, material distribution, and geometric features through digital slicing of a predefined model.

Currently, the predominant 3D printing technology used in the fabrication of MSRs is vat photopolymerization [20], [21]. Printing technologies in this category use a light source to cure photosensitive resin, enabling rapid fabrication of microstructures with high resolutions and compatibility with magnetic material doping. However, existing systems are largely limited to printing two-dimensional (2D) geometries, or at best, 3D geometric structures with 2D magnetization profiles [20], [21].

To address these limitations, the HeART Lab developed a fully automated stereolithography (SLA) based printing system capable of fabricating 3D geometric structures with programmable 3D magnetization directions [22]. SLA, a subset of vat photopolymerization, uses a precise light source, usually a laser or ultraviolet (UV) beam, to selectively cure photosensitive resin layer by layer, solidifying it into the desired shape. It has the advantage of high printing accuracy, precision, and the ability to create complex geometries [23].

This work optimizes the 3D printer and fabrication workflow previously developed, focusing on improving printing resolution and structural fidelity. First, improvements to the optical system are described in detail, including the adjustment to the type of light source, collimation system, and overall working principle. The new optical system is designed to eliminate conical solidification at the edge of the voxel and improve the curing accuracy. Then, a series of printing tests were conducted to increase the geometric

This work is supported by the Natural Sciences and Engineering Research Council of Canada (NSERC) through their Discovery Grant RGPIN-2024-06700, Canada Foundation for Innovation-John R. Evans Leaders Fund through grant 44508 and the McMaster Entrepreneurship Academy.

*Siwen Xie and Kaitlyn Clancy contributed equally to this work.

[1]Siwen Xie is with the Department of Computing and Software, McMaster University xies42@mcmaster.ca

[2]Kaitlyn Clancy is with the School of Biomedical Engineering, McMaster University clanck2@mcmaster.ca

[1,2]Onaizah Onaizah is with the Department of Computing and Software and the School of Biomedical Engineering, McMaster University, 1280 Main St. W., Hamilton, ON L8S 4L8, Canada onaizaho@mcmaster.ca

resolution to 803 μm from the previous 1.6 mm achieved at a layer height of 110 μm.

To validate the resolution of this printing system, a series of tests were conducted, demonstrating a process of accurately printing various structures including: 1) a beam for magnetization characterization, 2) a gripper to demonstrate grasping and translational capabilities, and 3) a 'HEART' sign highlighting improvements in voxel shape and size characteristics. Overall, this paper demonstrates that the optimized SLA-based 3D printing technology enables the fabrication of MSRs with submillimeter resolution, higher structural complexity, improved motion capabilities, and enhanced adaptability to application-specific tasks.

II. BACKGROUND

A. Magnetic Actuation

To understand the behavior and control of complex MSR structures, a brief review of the fundamental principles of magnetic actuation is provided. Common actuation systems consist of permanent magnets or electromagnetic coils to generate external magnetic fields. These systems exert forces and torque on objects with embedded magnetic materials, enabling remote manipulation.

A magnetic moment, $\mathbf{m}$, subjected to an external magnetic flux density, $\mathbf{B}$. experiences a torque, $\boldsymbol{\tau}$, which aligns the magnetic moment with the direction of the magnetic field. In addition, when the magnetic field is spatially varying or nonuniform, a net force, $\mathbf{F}$, is generated causing translational motion of the magnetic object. These interactions are mathematically governed by the following equations:

$$\boldsymbol{\tau} = \mathbf{m} \times \mathbf{B} \tag{1}$$

$$\mathbf{F} = \nabla(\mathbf{m} \cdot \mathbf{B}) \tag{2}$$

Assuming no free currents in the domain ($\nabla \times \mathbf{B} = 0$), Maxwell's equations can be applied to simplify the force equation as:

$$\mathbf{F} = [\mathbf{m} \cdot \frac{\partial \mathbf{B}}{\partial x}, \mathbf{m} \cdot \frac{\partial \mathbf{B}}{\partial y}, \mathbf{m} \cdot \frac{\partial \mathbf{B}}{\partial z}]^T \tag{3}$$

Therefore, the magnetic material will rotate to align with the magnetic field direction and then translate in the direction of the increasing magnetic field [24]. This concept is shown in Fig. 1. These equations serve as the foundation for analyzing, designing, and controlling MSRs.

External magnetic fields used for actuating MSRs can be generated using either permanent magnets or electromagnetic coil systems. Each approach has distinct advantages and limitations.

A single permanent magnet will inherently produce a nonuniform field resulting in a field gradient. This makes it suitable for navigation and guidance, as it can induce translational motion. In many basic systems, a single handheld permanent magnet is used to manipulate MSRs. The resulting field gradient is highly user-dependent based on their intuition and experience, leading to inconsistencies and limited repeatability [24].

More advanced systems incorporate multiple permanent magnet systems that are motor operated. One example is the Niobe system by Sterioaxis, which comprises of two large permanent magnets attached to rotational motors [24]. This system is primarily used in clinical settings for actuation of magnetic catheters and has demonstrated reliable directional control [24].

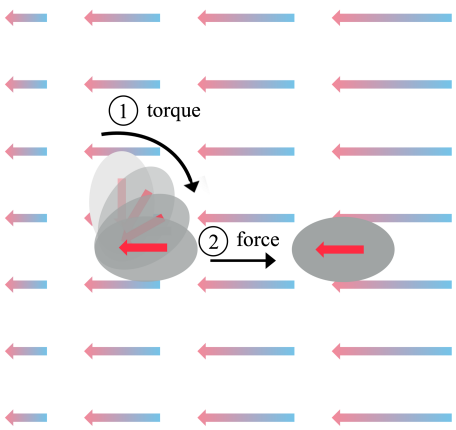

Fig. 1. The red arrow indicates the magnetization direction of the object. The object aligns with the magnetic field direction resulting in magnetic torque. Then the object translates in the direction of the increasing magnetic field resulting in a magnetic force. The gray ellipse represents the position and direction of this magnetic object at different time points. As time passes the ellipse becomes darker. The background arrows indicate the direction and strength of the external magnetic field, and the arrow length represents the magnetic field strength (decreasing from right to left).

On the other hand, electromagnetic coil systems offer enhanced precision and flexibility. However, they are often on the laboratory scale and require a lot of power that is lost to heat generation. These systems are capable of generating both uniform fields (using Helmholtz coil configuration) and field gradients (using Maxwell coil configuration) [24]. Helmholtz coil systems are used to generate torque, while Maxwell systems can produce linear magnetic gradients for constant velocity translational motion [24].

Electromagnetic coil systems provide more accurate actuation and precise control of magnets compared to handheld permanent magnet systems [24]. They also have the advantage of completely removing the magnetic field by turning off the current to the coils which can remove transient effects and provide a fail safe [24].

B. Printer Design

This paper covers the updated optical system of a fully automated SLA based polymerization printer. The printer was originally designed using a UV LED to cure voxels or 3D pixels. These voxels were 1.6 mm in diameter with a Gaussian energy distribution and curing profile across the voxel. The new updated optics system uses a LP405C1 laser diode along with a near ultraviolet (NUV) beam shaper to achieve evenly cured voxels 803 μm in diameter.

In order to print various designs, a COMSOL 6.2 multiphysics interface was used to build structures with predefined voxels. Each voxel is encoded with a magnetization direction using the 'Magnetic Fields, No Currents physics' package. Once the desired structure was modeled, a custom Java slicer software was created for an instruction set to be sent to the

printer. The slicer code sorts each voxel by their position within each layer and cures radially outward from the origin. The magnetization of each voxel is converted from cartesian data to spherical coordinates for the printer's magnetization motors. All of the data is then converted into the number of pulses per shaft resolution required by each motor and then the geometric magnetization code is exported as a comma-separated values (CSV) file. This file is read by the microcontroller during the printing process.

The printer is designed to translate the base plate in the x and y directions for curing the desired voxel. A permanent magnet is mounted on a dual rotating platform that can turn a full 360° along two planes to generate a local magnetic field with programmable orientation, achieving voxel-level magnetization in 3D directions. Then, from below the resin tank, the laser selectively cures the desired voxel to lock in the local magnetization direction. This process repeats voxel by voxel and then layer by layer until the whole structure is complete. The overall process is outlined in Fig. 2.

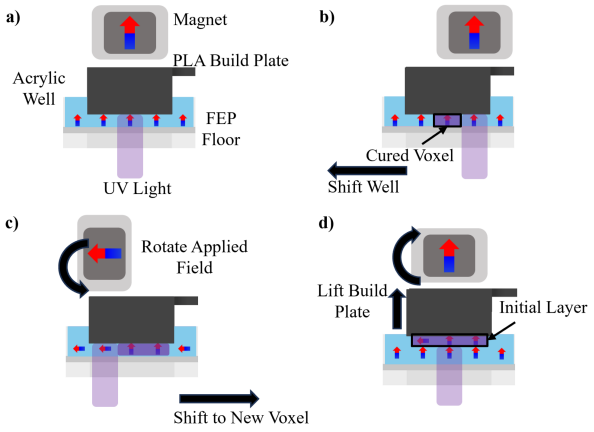

Fig. 2. Printing Process. **a)** First voxel is cured. **b)** The well is translated to the next voxel and the curing process repeats. **c)** Magnet is reoriented to cause simultaneous alignment of the magnetic particles within the resin well. The voxel is selectively cured to lock in the magnetization. **d)** Delamination of the first layer adhered to the build plate and the start of the second layer curing process begins.

III. METHODS

A. Assembly of the 3D printer

This work replaces the optical system and performs structural design improvements on an existing 3D printer [22], as shown in Fig. 3. The original optics include a UV LED and a related printed circuit board (PCB). In this work, the optical system was upgraded to higher precision components, including Compact Laser Diode/Temperature Controller with Mount (CLD1010LP, Thorlabs, USA), Pigtailed Laser Diode with Collimator (LP405C1, Thorlabs, USA), Near Ultraviolet (NUV) Flat Top Beam Shaper πShaper_6_6, AdlOptica, Germany), and Fused Silica Broadband Dielectric Mirror (BB1-E01, Thorlabs, USA). The integrated settings of the Compact Laser Diode/Temperature Controller with Mount include temperature settings of 25°C, current settings of 40 mA, and power settings of 0.003 mW to ensure the stability of the laser diode and the efficient output of the light source.

The overall structure of the 3D printer consists of several parts as follows. For the printing process, two stepper motors

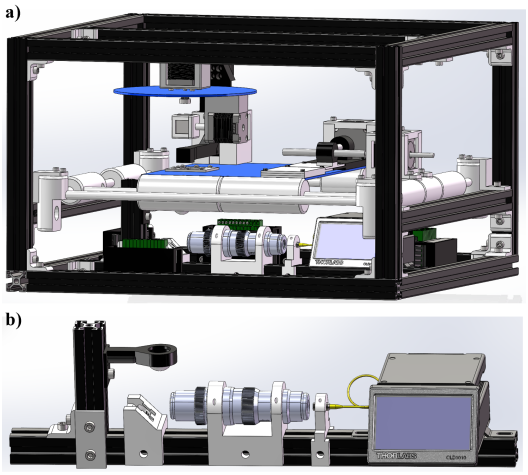

Fig. 3. Updated design of the 3D printer. **a)** Assembly of the 3D printer including the new components. **b)** Assembly of the updated optical system for higher resolution printing.

(Nema 17, Motion Control Products Ltd., China) are used with magnetic encoders to precisely control the rotation of the permanent magnets through a driver (TB6600, COVVY, USA). The θ-motor controls the movement of the acrylic plate in the x-y plane, while the φ-motor directly rotates the magnet in the y-z plane. The base of the build platform is laser cut from an acrylic plate (3mm, SimbaLux, USA) and fixed to ultra-straight rods using linear bearings to ensure stable movement. For precise positioning of the resin well, three stepper motors (Nema 23, Motion Control Products Ltd., China) are mounted on a 3D printed housing unit (MK4S, Prusa Research, Czechia) with stainless steel threaded rods (3M right-hand thread, 0.5 mm pitch, Uxcell, Philippines). The z-motor drives the build plate arm to ensure that its surface is parallel to the bottom of the resin tank for uniform curing. The resin well consists of two acrylic plates sandwiching a thin FEP film, which are fixed by nylon screws. The bottom acrylic plate has an optical opening to minimize laser refraction. A Raspberry Pi microcontroller (SC0022, Mouser Electronics, USA) drives the stepper motor and the optical system, and current regulation is accomplished through a constant current driver (NCR420ZX, Digikey, USA) and a 10 Ω resistor.

B. Printing Materials

For the fabrication of MSRs in this work, a composite material was prepared using hard magnetic particles (NdFeB, Nanochemazone, Canada) and a commercial photosensitive printing resin (ENGR-E38L, 3D Materials Co., Ltd., South Korea). The above materials were mixed in the desired mass ratio using a precision scale (PCE-BSH 6000, PCE Instruments, Canada). This UV resin has a shore hardness of 60A and 150% elongation at break, which is desirable for fabricating flexible structures with repeated deformation capabilities. The mixture was then thoroughly stirred to ensure homogeneous dispersion of magnetic particles within the resin matrix. This results in consistent magnetic and mechanical properties throughout the printed structures.

After mixing, the composite material was transferred to the resin well of the printer. Once the printing process was

complete, the fabricated structures were removed from the build plate using a razor and washed with 99% isopropyl alcohol (IPA, Rapid Protectant, Canada) to remove excess uncured resin.

IV. RESULTS

A. Voxel Testing

To determine the optimal curing time, a 1:2 mass ratio of NdFeB magnetic particles to elastic resin was used to create the composite material. This material was then cured at intervals of 0.1 s for times ranging from 0.3 s to 1 s and the results were analyzed. The curing time was chosen based on the overall shape and size of the voxel that closely matched the shape and resolution of the current laser diode spot size. The spot size obtained from all cure times were imaged using a camera (ACE CMOS, Basler, USA). The spot size with a perfect circular voxel and the same diameter as the laser diode spot size was found to occur at a curing time of 0.5 s and resulted in a resolution of 803 μm in diameter.

B. HEART Sign Testing

Given the NUV beam shaper was selected to generate voxels with an even energy distribution, a HEART sign was designed using COMSOL to demonstrate this new capability. This sign is composed of 52 magnetic voxels with an overall size of 15.257 mm by 4.015 mm and two layers of 220 μm height. First a layer of clear resin was cured to the build plate. The excess uncured resin was then washed off using an IPA solution, dried, and replaced into a new well filled with a 1:2 ratio of magnetic particles to resin. Voxels designed to create HEART letters were then cured on top. To show a 3D aspect of the printer, the letters were uniformly magnetized and an image of the magnetic flux across a single plane was captured from the Magview (cmos-magview S, Matesy GmbH, Germany). The printed HEART sign is shown in Fig. 4.

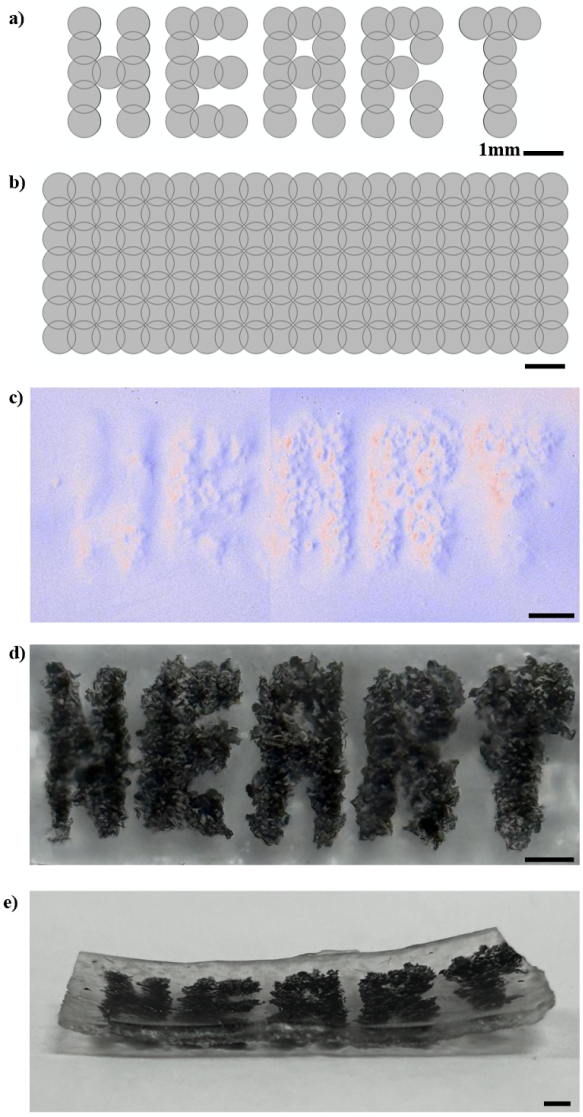

Fig. 4. HEART sign. **a)** Modeled HEART sign in COMSOL with the composite material and **b)** Modeled HEART sign in COMSOL with the addition of the elastic resin. **c)** Printed HEART sign image captured from the Magview shows the magnetization directions of the voxels. **d)** Camera image of the printed HEART sign. **e)** The thickness of the HEART sign shows multi-layer printing structure.

C. Beam Bending Analysis

A beam was designed and uniformly magnetized to validate the magnetization directions from the 3D printer of the new high resolution MSRs. The beam was designed to be 7 voxels (5.621 mm) in length and 1 voxel (0.803 mm) wide. The magnetization direction remains consistent throughout the beam structure, oriented in the horizontal direction. Once fabricated, a coil system was used to generate an external magnetic field to deflect the beam. The electromagnetic coil system consists of 3 pairs of coil for each respective axis set up to approximate a Helmholtz configuration. The current to the coils is controlled through 3 analog servo drives (AB50A200I, Advanced Motion Controls, USA) which has its own power supply (PS50A, Advanced Motion Controller, USA). The control signal for the servo drives is sent through a digital-to-analog converter (Model 826, Sensoray, USA) connected to a computer running a custom program. The desired magnetic flux density is entered into this program.

In this test, a magnetic field was applied perpendicular to the beam's magnetization direction at intervals of 2.5 mT ranging from -20 mT to 20 mT. The field is measured using a Teslameter (F71 Teslameter, Lake Shore Crytronics, USA). Images at discrete time points are captured while the magnetic field is used to deflect the beam. The results and analysis of the bending along with the overall design are shown in Fig 5. The deflection angle of the beam exhibits a nonlinear relationship with the applied magnetic field strength, characterized by a linear response region from approximately -5 mT to 5 mT and saturation behavior for $|\mathbf{B}| > 15$ mT when the magnetic field direction aligns with the magnetization direction. The results show that for a single magnetization mode, the beam structure exhibits a good magnetic and material response. The beam deflection test was recorded and can be seen in the Supplementary Video.

D. Gripper Analysis

To verify the capability of the optimized printer to fabricate MSRs with complex structures and functions, two flexible microgrippers were designed and printed. The '+'

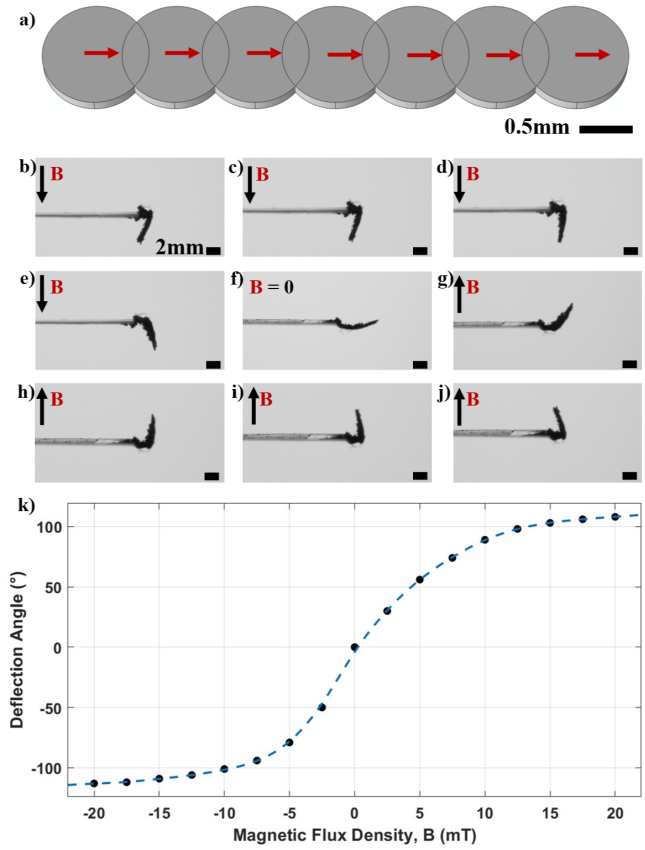

Fig. 5. Beam Analysis. **a)** Modeled beam in COMSOL and the red arrows show the uniform magnetization direction of the beam. **b)** - **j)** Deflection images as the beam bends under an applied magnetic field strength of -20, -15, -10, -5, 0, 5, 10, 15, and 20 mT (positive field points upward). **k)** Graph of the deflection angle as a function of the magnetic flux density, **B**.

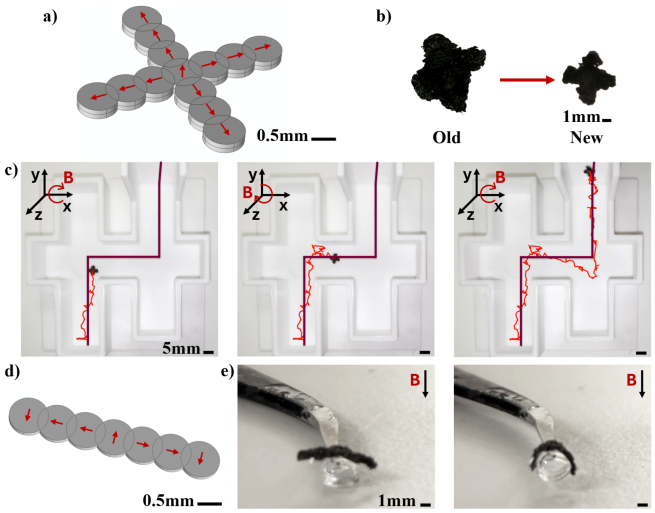

Fig. 6. Gripper Analysis. **a)** Modeled '+' shaped gripper in COMSOL with the red arrows showing the magnetization direction of each voxel. **b)** The '+' shaped gripper size change from the old and new optics system. **c)** The '+' shaped gripper travels through the maze and climbs the wall, it is shown at three time points. **d)** Modeled line-shaped gripper in COMSOL with the red arrows showing the magnetization direction of each voxel. **e)** The line-shaped gripper grabs an object.

shaped gripper design focused on crawling and climbing across a maze, while the line-shaped gripper focused on grasping an object. The line design was created to allow for clear observations of grasping abilities. Fig. 6. a) shows the initial design of the '+' shaped gripper and the 3D magnetization direction distribution inside it. The voxel-level magnetic encoding allowed it to move under a rotating magnetic field. The gripper consists of multiple voxels with varying magnetization. After printing, the structure was washed in IPA. Then it was added to the testing platform for performance verification. Fig. 6. b) shows the improvement in accuracy compared to the previous printing technology. Fig. 6. c) shows the gripper's motion and climbing behavior under a rotating magnetic field, manually generated by a permanent magnet. The gripper advances by rolling and results in changes in motion direction when the magnetic field orientation changes. Fig. 6. d) shows the initial design of the line-shaped gripper and the 3D magnetization distribution of the voxels. The voxel-level magnetic encoding allowed the gripper pick up small light-weight objects as shown in Fig. 6. e). The full video showing both gripper capabilities can be seen in the Supplementary Video.

V. DISCUSSION

The upgraded optics system uses the LP405C1 laser diode, which has advantages such as long-term service life and improved output power stability compared to the previously used UV LED. Theoretically, this system can achieve voxels with a resolution as small as 50 μm based on past simulations; however, in this work, the achievable printing resolution is limited to 803 μm. Multiple optical factors cause this difference. First, the πShaper 6_6 beam shaper is sensitive to alignment errors. Although it can provide a uniform flat-top light intensity distribution, it has high requirements for angles and lateral offsets. Small errors can cause beam distortion, uneven curing, and voxel deformation. The current optical path may not be optimal for minimizing spot size. Future improvements should take this into consideration along with the use of different lenses better suited for focusing the beam to a smaller square spot size. Furthermore, the curing process is heavily influenced by the permanent magnet. The permanent magnet must be a specific distance from the well for neutral buoyancy of the magnetic particles. Magnetic field strengths that are too strong or weak cause errors in light penetration depth, ultimately affecting the accuracy and consistency of the magnetic voxels.

In addition to the optical parts, the mass ratio of magnetic particles to UV polymer limits the curing resolution. High concentrations of magnetic particles will affect the optical transparency of the mixed resin and reduce the curing depth and uniformity. The optical and chemical properties of the UV polymer may also influence the minimum achievable spot size. Future work should explore a variety of UV polymers to obtain faster reaction rates, higher absorption efficiency, and more accurate curing of voxels. Future research will systematically address these issues to narrow the gap between theoretical resolution and actual printing accuracy.

VI. CONCLUSIONS

This research optimized an existing SLA-based 3D printer, achieving higher curing accuracy and structural resolution

by upgrading the optical system from UV LED to a laser-based configuration and enhancing the collimation and beam shaping capabilities. Performance evaluation showed that the system can print complex microstructures, including the HEART sign and functional magnetic microgrippers and beams, with high fidelity and achieve reliable magnetization direction control.

Looking ahead, future enhancements to the 3D printing system will focus on multi-material integration, aiming to fabricate MSRs embedded with more than one functional material. Furthermore, MSRs with integrated flexible electronics that can be fully-printed would open up new possibilities in the fields of biomedical sensing, active control, and intelligent *in vivo* operations.

ACKNOWLEDGMENT

The authors would like to acknowledge Veerash Palanichamy and Shivam Gupta for all their help with the experimental setup and aiding in the use of the coil system.

REFERENCES

[1] M. Ussia, M. Urso, C. Oral, X. Peng, and M. Pumera, "Magnetic microrobot swarms with polymeric hands catching bacteria and microplastics in water," *ACS nano*, vol. 18, 05 2024.

[2] M. Sitti and D. Wiersma, "Pros and cons: Magnetic versus optical microrobots," *Advanced Materials*, vol. 32, p. 1906766, 02 2020.

[3] X. Liang, Y. Zhao, D. Liu, Y. Deng, T. Arai, M. Kojima, and X. Liu, "Magnetic microrobots fabricated by photopolymerization and assembly," *Cyborg and Bionic Systems*, vol. 4, 11 2023.

[4] L. Hines, K. Petersen, G. Z. Lum, and M. Sitti, "Soft actuators for small-scale robotics," *Advanced Materials*, vol. 29, no. 13, p. 1603483, 2017.

[5] N. Xia, B. Jin, D. Jin, Z. Yang, C. Pan, Q. Wang, F. Ji, V. Iacovacci, C. Majidi, Y. Ding, and L. Zhang, "Decoupling and reprogramming the wiggling motion of midge larvae using a soft robotic platform," *Advanced Materials*, vol. 34, p. 2109126, 03 2022.

[6] Y. Kim, H. Yuk, R. Zhao, S. Chester, and X. Zhao, "Printing ferromagnetic domains for untethered fast-transforming soft materials," *Nature*, vol. 558, pp. 274–279, 06 2018.

[7] J. Chen, D. Jin, Q. Wang, and X. Ma, "Programming ferromagnetic soft materials for miniature soft robots: Design, fabrication, and applications," *Journal of Materials Science Technology*, vol. 219, 09 2024.

[8] N. Xia, D. Jin, and L. Zhang, "Magnetic soft matter toward programmable and multifunctional miniature machines," *Accounts of Materials Research*, vol. 5, 01 2024.

[9] R. Soon, Z. Yin, M. Dogan, N. Dogan, M. Tiryaki, A. Karacakol, A. Aydin, P. Esmaeili-Dokht, and M. Sitti, "Pangolin-inspired untethered magnetic robot for on-demand biomedical heating applications," *Nature Communications*, vol. 14, 06 2023.

[10] Y. Sun, W. Zhang, J. Gu, L. Xia, Y. Cao, X. Zhu, H. Wen, S. Ouyang, R. Liu, J. Li, Z. Jiang, D. Cheng, Y. Lv, X. Han, W. Qiu, K. Cai, E. Song, Q. Cao, and L. Li, "Magnetically driven capsules with multimodal response and multifunctionality for biomedical applications," *Nature Communications*, vol. 15, pp. 1–14, 02 2024.

[11] C. Zhou, Y. Yang, J. Wang, Q. Wu, Z. Gu, Y. Zhou, X. Liu, Y. Yang, H. Tang, Q. Ling, L. Wang, and J. Zang, "Ferromagnetic soft catheter robots for minimally invasive bioprinting," *Nature Communications*, vol. 12, 08 2021.

[12] Y. Deng, Y. Zhao, J. Zhang, T. Arai, Q. Huang, and X. Liu, "Fabrication of magnetic microrobots by assembly," *Advanced Intelligent Systems*, vol. 6, 11 2023.

[13] M. Manian, M. Cardona, R. Yuan, M. Clark, D. Kagan, S. Balasubramanian, and J. Wang, "Template-assisted fabrication of salt-independent catalytic tubular microengines," *ACS nano*, vol. 4, pp. 1799–804, 03 2010.

[14] W. Gao, S. Sattayasamitsathit, M. Manian, D. Weihs, and J. Wang, "Magnetically powered flexible metal nanowire motors," *Journal of the American Chemical Society*, vol. 132, pp. 14403–5, 09 2010.

[15] V. Sridhar, B.-W. Park, and M. Sitti, "Light-driven janus hollow mesoporous tio2–au microswimmers," *Advanced Functional Materials*, vol. 28, no. 25, p. 1704902, 2018.

[16] X. Ma, S. Jang, M. Popescu, W. Uspal, A. López, K. Hahn, D. Kim, and S. Sanchez, "Reversed janus micro/nano-motors with internal chemical engine," *ACS nano*, vol. 10, 09 2016.

[17] Z. Wu, X. Lin, Y. Wu, T. Si, J. Sun, and Q. He, "Near-infrared light-triggered "on/off" motion of polymer multi layer rockets," *ACS nano*, vol. 8, 05 2014.

[18] H. Wang and M. Pumera, "Micro/nanomachines and living biosystems: From simple interactions to microcyborgs," *Advanced Functional Materials*, vol. 28, p. 1705421, 06 2018.

[19] M. Sitti, "Microscale and nanoscale robotics systems [grand challenges of robotics]," *Robotics Automation Magazine, IEEE*, vol. 14, pp. 53 – 60, 04 2007.

[20] Z. Li, Y. Lai, and E. Diller, "3d printing of multilayer magnetic miniature soft robots with programmable magnetization," *Advanced Intelligent Systems*, vol. 6, 05 2023.

[21] Y. Huang, H. Sun, C. Zhang, R. Gao, H. Shen, and P. Zhao, "Multi-material magnetic field-assisted additive manufacturing system for flexible actuators with programmable magnetic arrangements," *Frontiers of Mechanical Engineering*, vol. 19, 05 2024.

[22] J. Sholdice, K. Clancy, K. Teresinska, C. Castro, L. Watson, and O. Onaizah, "Automated fabrication of 3d printed magnetic soft robots with programmable 3d magnetizations," *Advanced Robotics Research*, 02 2025.

[23] A. Husna, S. Ashrafi, A. N. M. A. Tomal, N. T. Tuli, and A. Rashid, "Recent advancements in stereolithography (sla) and their optimization of process parameters for sustainable manufacturing," *Hybrid Advances*, vol. 7, p. 100307, 10 2024.

[24] Z. Yang and L. Zhang, "Magnetic actuation systems for miniature robots: A review," *Advanced Intelligent Systems*, vol. 2, p. 2000082, 06 2020.